Article

Cell Reports

Synucleins Have Multiple Effects on Presynaptic Architecture

Graphical Abstract

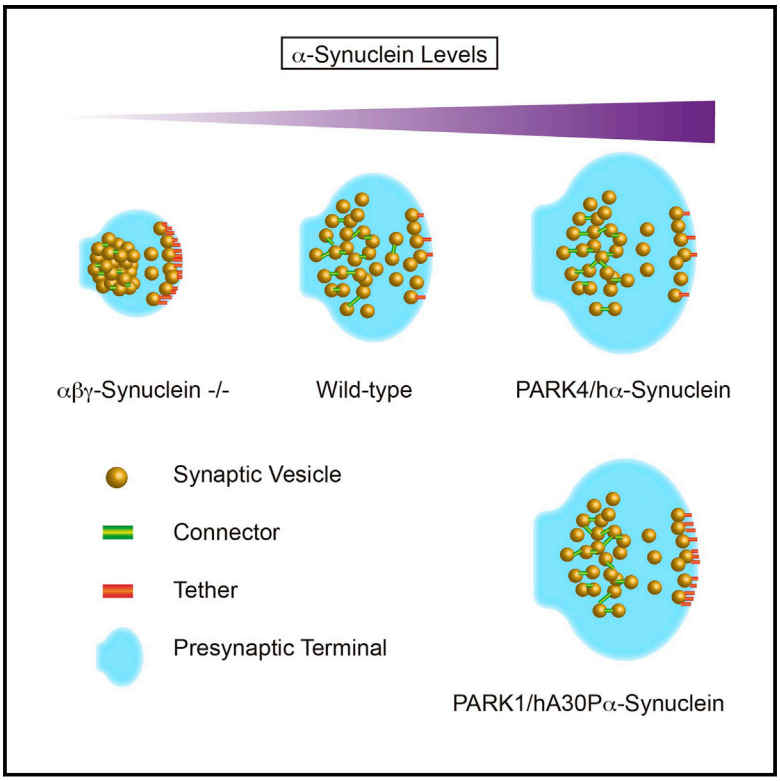

Authors

Karina J. Vargas, Nikolas Schrod, Taylor Davis, ..., Ulrike Laugks, Vladan Lucic, Sreeganga S. Chandra

Correspondence

vladan@biochem.mpg.de (V.L.), sreeganga.chandra@yale.edu (S.S.C.)

In Brief

Synucleins (α, β, γ-synuclein) are abundant presynaptic proteins, with α-synuclein linked to the pathogenesis of Parkinson's disease. Vargas et al. investigate the effects of deleting synucleins and overexpressing mutated α-synuclein on synapse architecture using electron microscopy. They find that synucleins regulate presynaptic terminal size and synaptic vesicle distribution.

Highlights

- Synucleins are determinants of synapse size
- Connectors and tethers are altered in αβγ-synuclein−/−
- PARK mutations primarily affect tethering of synaptic vesicles
- Phospho-amphiphysin-2 may constitute connectors linking synaptic vesicles

Vargas et al., 2017, Cell Reports *18*, 161–173
January 3, 2017
http://dx.doi.org/10.1016/j.celrep.2016.12.023

Cell Reports
Article

Synucleins Have Multiple Effects on Presynaptic Architecture

Karina J. Vargas,[1,2,7] Nikolas Schrod,[3,7] Taylor Davis,[1,2] Ruben Fernandez-Busnadiego,[2,4,5] Yumiko V. Taguchi,[2,4] Ulrike Laugks,[3] Vladan Lucic,[3,*] and Sreeganga S. Chandra[1,2,6,8,*]
[1]Department of Neurology
[2]Program in Cellular Neuroscience, Neurodegeneration and Repair
Yale University, New Haven, CT 06536, USA
[3]Max Planck Institute of Biochemistry, Am Klopferspitz 18, 82152 Martinsried, Germany
[4]Department of Cell Biology
[5]Howard Hughes Medical Institute
School of Medicine, Yale University, New Haven, CT 06510, USA
[6]Department of Neuroscience, Yale University, New Haven, CT 06519, USA
[7]Co-first author
[8]Lead Contact
*Correspondence: vladan@biochem.mpg.de (V.L.), sreeganga.chandra@yale.edu (S.S.C.)
http://dx.doi.org/10.1016/j.celrep.2016.12.023

SUMMARY

Synucleins (α, β, γ-synuclein) are a family of abundant presynaptic proteins. α-Synuclein is causally linked to the pathogenesis of Parkinson's disease (PD). In an effort to define their physiological and pathological function or functions, we investigated the effects of deleting synucleins and overexpressing α-synuclein PD mutations, in mice, on synapse architecture using electron microscopy (EM) and cryoelectron tomography (cryo-ET). We show that synucleins are regulators of presynapse size and synaptic vesicle (SV) pool organization. Using cryo-ET, we observed that deletion of synucleins increases SV tethering to the active zone but decreases the inter-linking of SVs by short connectors. These ultrastructural changes were correlated with discrete protein phosphorylation changes in αβγ-synuclein−/− neurons. We also determined that α-synuclein PD mutants (PARK1/hA30P and PARK4/hα-syn) primarily affected presynaptic cytomatrix proximal to the active zone, congruent with previous findings that these PD mutations decrease neurotransmission. Collectively, our results suggest that synucleins are important orchestrators of presynaptic terminal topography.

INTRODUCTION

Synapses are exquisite examples of the axiom "form follows function." Subtle alterations in synapse structure can have profound functional consequences (Atasoy et al., 2007; Ho et al., 2003; Altrock et al., 2003; Gundelfinger et al., 2016; Jiang and Ehlers, 2013). This is underscored by many neurological and psychiatric illnesses being associated with alterations in synapse structure (van Spronsen and Hoogenraad, 2010; Penzes et al., 2011).

The presynaptic terminal has a complex architecture, with synaptic vesicles (SVs) located at different distances from the active zone (AZ) and functionally organized in three main pools: reserve, recycling, and readily releasable pool. Cryoelectron tomography (cryo-ET) has been used for the visualization of SV-interacting proteins because of its superior preservation of labile structures. Short filaments tethering SVs to the AZ, known as tethers, and filaments linking SVs to one another, known as connectors, were shown by cryo-ET to be the most prominent elements of the presynaptic cytomatrix. Tethers and connectors play important roles in controlling the distribution of SVs and the vesicle progression toward release (Fernández-Busnadiego et al., 2010, 2011). However, the proteins that regulate presynaptic structure, supramolecular organization, and canonical SV distribution, especially the molecular constituents of tethers and connectors, are not well defined, even though the presynaptic proteome has been cataloged (Takamori et al., 2006; Wilhelm et al., 2014) and molecular functions have been assigned to a large fraction of proteins.

Synucleins are a family of abundant presynaptic proteins (α, β, and γ-synuclein). They are 14 kDa proteins, with conserved N termini that bind acidic lipids and divergent C termini (Vargas and Chandra, 2015). Synucleins can sense and generate membrane curvature (Westphal and Chandra, 2013; Middleton and Rhoades, 2010), and this property implies functions in SV exocytosis or endocytosis (Merrifield and Kaksonen, 2014; Martens et al., 2007; Hui et al., 2009), the two steps that require membrane curvature. We previously showed that a conserved function of the synuclein family is to regulate the kinetics of SV endocytosis (Vargas et al., 2014). In addition, the literature supports a role for α-synuclein in SV exocytosis (Burré et al., 2010). These properties suggest that synucleins are likely to have an impact on presynaptic structure.

Mutations in the α-synuclein gene cause familial Parkinson's disease (PD), including six point mutations (A30P, E46K, H50Q,

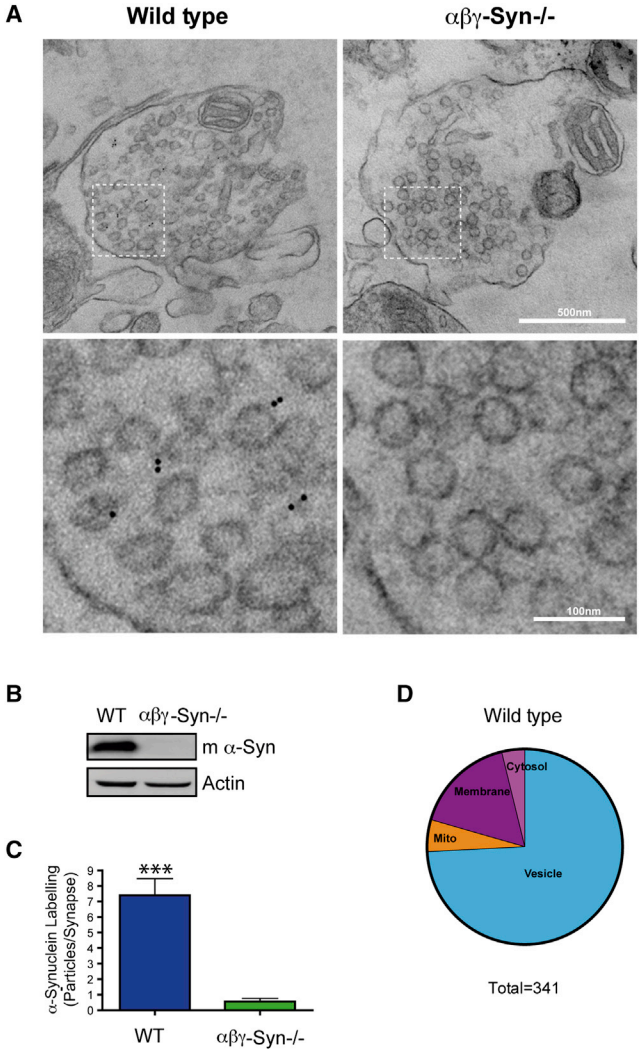

Figure 1. Synucleins Are Peripheral SV-Associated Proteins

(A) Representative electron micrographs of wild-type and αβγ-Syn−/− synaptosomes after hypotonic fixation and immuno-EM with an α-synuclein-specific antibody and secondary gold particles (top panels; scale bar, 500 nm). The bottom panels are zoomed-in regions noted in the top panels (scale bar, 100 nm). The black dots denote the locations of the gold particles.

(B) Western blotting of wild-type and αβγ-Syn−/− synaptosomes with a mouse α-synuclein antibody to confirm genotypes.

(C) Quantification of α-synuclein labeling in micrographs such as shown in (A). n = two experiments; 46–25 synapses per two to three mice per genotype. ***$p < 0.001$.

(D) Pie chart of the localization of α-synuclein gold particles (n = 341).

All data are presented as mean ± SEM.

G51D, A53T, and A53E—PARK1) (Polymeropoulos et al., 1997) and gene multiplications (duplication and triplication—PARK4) (Singleton et al., 2003). Moreover, sequence variants that enhance α-synuclein expression increase the risk for developing PD. In addition, α-synuclein is the main component of Lewy bodies, the signature pathology of PD, prompting many to consider α-synuclein as the key gene in the pathophysiology of PD. As with other neurodegenerative diseases, synapse dysfunction and loss are early events in the pathogenesis of PD (Calo et al., 2016; Bellucci et al., 2016); therefore, there is great interest in understanding how α-synuclein and its pathological variants affect synaptic structure and function.

To understand how synucleins influence synapse structure, we performed conventional electron microscopy (EM), immunoelectron microscopy (immuno-EM), and cryo-ET on wild-type (WT), synuclein null (αβγ-Syn−/−), and α-synuclein PD mutant (PARK1/human A30P [hA30P] and PARK4/human α-synuclein [hα-syn]) overexpressing synaptosomes and neurons. Through these different modes of visualization, we discovered that synucleins are important regulators of synapse size, as well as SV distribution. We also determined that PD mutants have select effects on the presynaptic cytomatrix.

RESULTS

Synucleins Are Associated with SVs throughout the Terminal

Synucleins are highly abundant at presynaptic termini (Nakajo et al., 1996; Westphal and Chandra, 2013; Wilhelm et al., 2014). In standard biochemical fractionation experiments, synucleins appear to be mainly cytosolic and absent from the SV fraction (Takamori et al., 2006). This is due to the characteristic of synucleins to come off the membrane in low ionic conditions. Fractionation experiments that preserve physiological salt conditions suggest synucleins are SV-associated proteins. To investigate the native distribution of synucleins in the physiological setting of the presynaptic terminal, we purified synaptosomes, quickly fixed them, and then carried out immuno-EM (Figure 1A) (De Camilli et al., 1983). As a positive control, we tested the location of the SV protein synaptobrevin 2 and found that 82.2% of the gold particles were found on SVs and 11.6% were found on the synaptic membrane. To confirm the specificity of the α-synuclein antibody, we stained αβγ-Syn−/− synaptosomes. There was a minimal background signal (Figure 1C) on mitochondria and synaptic plasma membrane but none on SVs. When we probed for the localization of α-synuclein in wild-type synaptosomes, the majority of the labeling, 74.2% of gold particles were found on SVs and 16.7% were found on the synaptic membrane (Figures 1C and 1D). This is consistent with previously published EM images localizing α-synuclein to SVs (Clayton and George, 1999; Boassa et al., 2013). From these electron micrographs, we conclude that under native conditions, a significant fraction of α-synuclein is associated with SVs and found throughout the terminal (Figure 1). Biophysical studies have shown that synucleins have high affinity for curved membranes, with the strongest binding to 40–50 nm vesicles (Middleton and Rhoades, 2010). This is the precise diameter range of SVs, and our findings can thus be explained by this biophysical property of synucleins.

Deletion of Synucleins Results in Smaller Presynaptic Termini

To examine whether deletion of synucleins results in structural alterations, in addition to the documented vesicle cycling deficits (Burré et al., 2010; Vargas et al., 2014), we performed conventional EM on wild-type and αβγ-Syn−/− dissociated

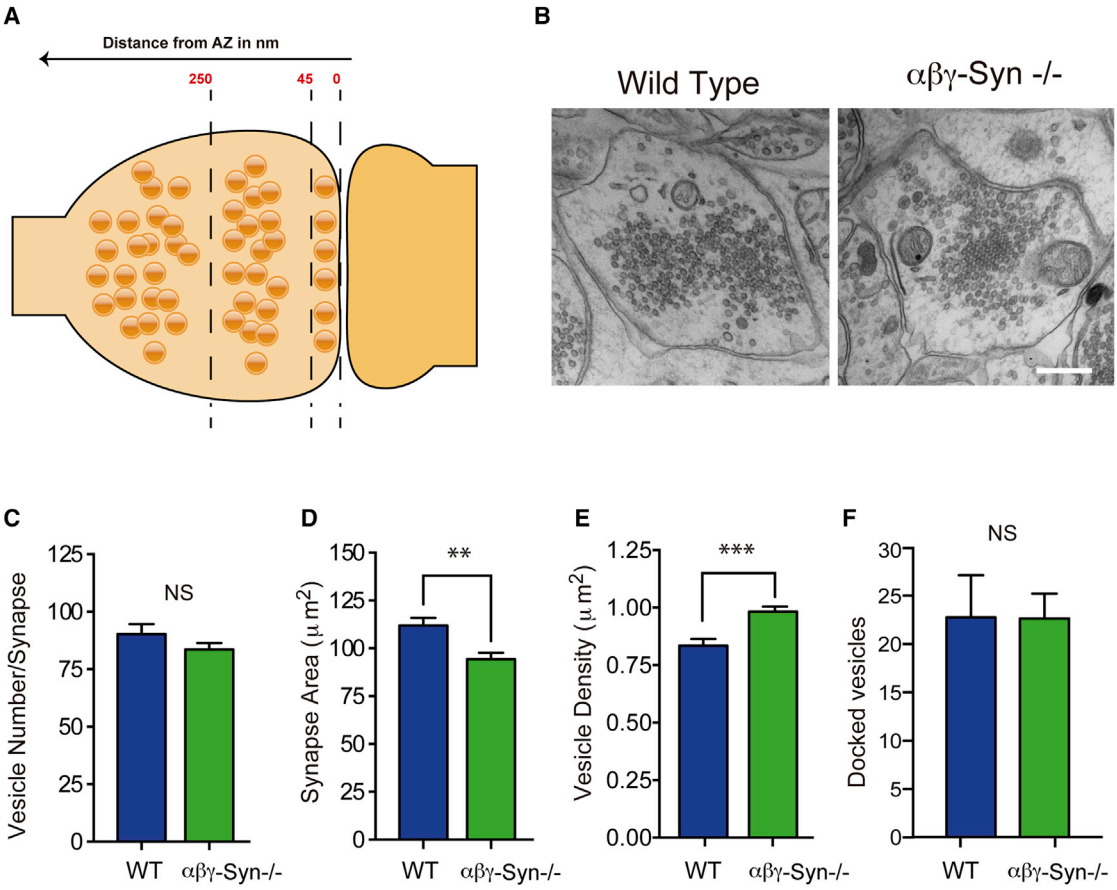

Figure 2. EM of Wild-Type and αβγ-Syn−/− Synapses

(A) Cartoon of a wild-type synapse with the three zone of SVs indicated: 45 nm from AZ, docked or proximal SVs; 45–250 nm, intermediate SVs; >250 nm, distal SVs.

(B) Electron micrograph of wild-type and αβγ-Syn−/− synapses.

(C–F) Quantification in wild-type (blue) and αβγ-Syn−/− (green) synapses of (C) SV number, (D) presynaptic terminal area, (E) SV density per presynaptic area, and (F) docked vesicle number.

n = 3 independent cultures, with a minimum of 56 micrographs per neuronal culture. n = 3 independent neuronal cultures; 50–150 synapses per genotype per culture were analyzed. Scale bar for (B), 400 nm. NS, not significant. **p < 0.01, ***p < 0.001.

All data are presented as mean ± SEM.

hippocampal neuronal cultures (Figure 2). In wild-type CA1 hippocampal neurons in culture, the average presynaptic terminal area was 112 μm^2 and has on average 90 vesicles per bouton, consistent with literature (Figures 2C and 2D) (Greten-Harrison et al., 2010). These features are altered when synucleins are absent. In αβγ-Syn−/− neurons, the mean presynaptic area is decreased by ~16% to 94 μm^2 (Figure 2C) while maintaining the number of SVs (Figure 2D). Consequently, SV density is increased relative to the wild-type (Figure 2E). The same phenotype was observed in brain tissue, specifically in CA1 and CA3 regions of the hippocampus (Greten-Harrison et al., 2010), strongly suggesting that this phenotype is cell autonomous.

In wild-type synapses, SV distribution is not homogeneous and three SV pools have been defined both functionally and spatially in reference to the AZ. Docked or proximal vesicles are found adjacent to the AZ (Figures 2A and 2B). In high-pressure frozen and freeze-dehydrated samples, docked vesicles that are attached to the plasma membrane at the AZ constitute the readily releasable pool (RRP) that is primed for release (Figures 2A and 2B) (Imig et al., 2014). The recycling pool is used to sustain normal neurotransmission, while the reserve pool is used under conditions of high stimulation. The recycling and reserve pool SVs are recognized to be interspersed, though the reserve pool, which makes up most of the total SV pool, is physically located more distally (Rizzoli and Betz, 2005). To investigate by EM the organization of SVs from a structural standpoint, the presynaptic terminal was divided into three regions: 0–45 nm, 45–250 nm, and >250 nm from AZ (Figure 2A). We characterized the overall distribution of SVs in wild-type and αβγ-Syn−/− synapses by both EM and cryo-ET. In the case of cryo-ET, as in previous studies, a 250 nm limit was imposed because of the large variability of the number of SVs and the decreased image contrast beyond that distance. By conventional EM, we observe that wild-type and αβγ-Syn−/− synapses

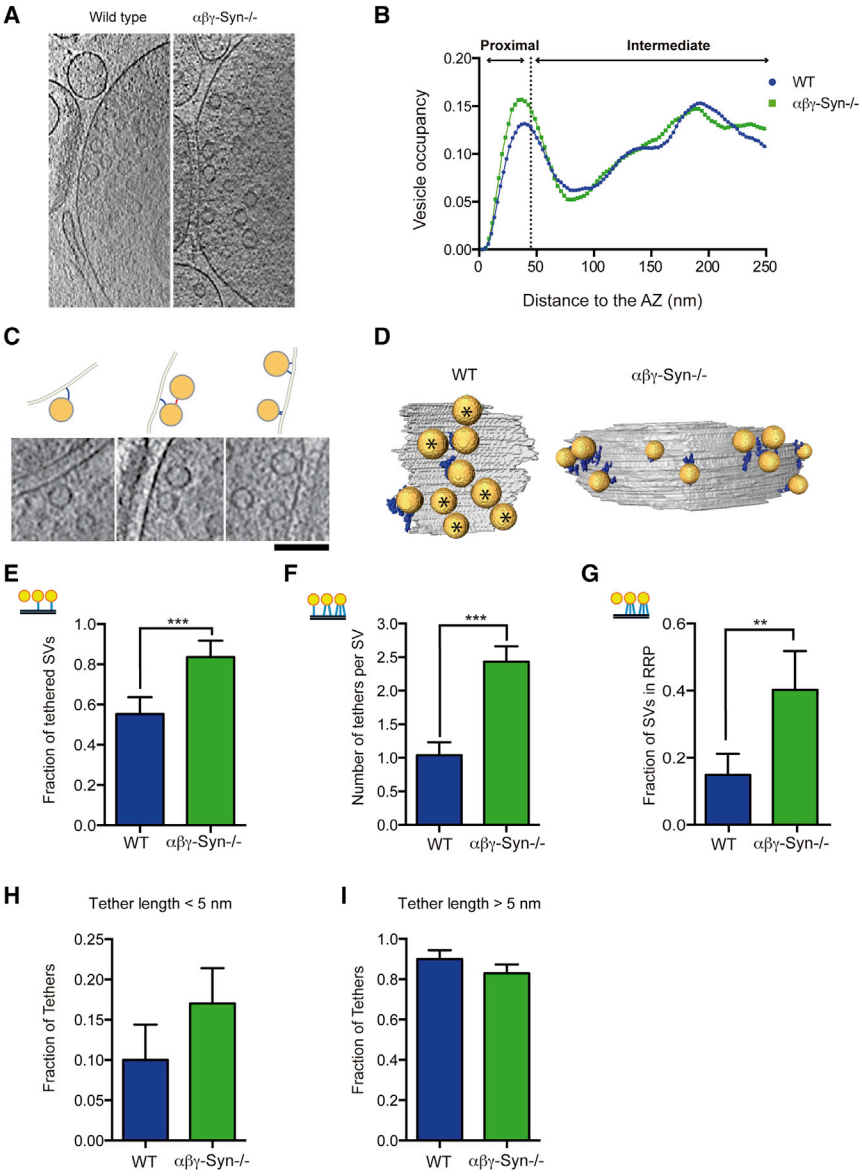

Figure 3. Cryo-ET of Wild-Type and αβγ-Syn−/− Synapses Reveals Increased Tethering upon Deletion of Synucleins

(A) Representative computationally extracted 2-nm-thick cryo-ET slices of wild-type and αβγ-Syn−/− synaptosomes.

(B) SV distribution calculated as the fraction of cytoplasmic volume occupied by SVs in the first 250 nm from the AZ.

(C) Examples of tethered SVs, along with line diagrams of images. Computationally extracted tomographic slices are 2 nm thick. Scale bar, 100 nm.

(D) 3D visualization of SVs (yellow), tethers (blue), and AZ (gray). Asterisks are proximal vesicles that are not tethered.

(E) Fraction of proximal SVs that have at least one tether in wild-type and αβγ-Syn−/−.

(F) Mean number of tethers per proximal SV per synapse in the two genotypes. $p < 0.001$ by Kruskal-Wallis (K-W) test.

(G) Fraction of proximal SVs with two or more tethers (structural RRP). $p < 0.01$ by χ^2 test.

(H) Fraction of tethers shorter than 5 nm.

(I) Fraction of tethers longer than 5 nm.

All data are presented as mean ± SEM. n = 3 independent experiments. **p < 0.01, ***p < 0.001.

have a similar SV distribution (Figures 2A and 2B). SVs were visible in all three regions in αβγ-Syn−/− synapses, even though they are smaller. By cryo-ET, the overall number and distribution of SVs in the first 250 nm from the AZ were also similar in wild-type and αβγ-Syn−/− (Figures 3A and 3B).

Alterations in Presynaptic Cytomatrix of Synapses Lacking Endogenous Synucleins

We systematically characterized presynaptic, ultrastructural elements starting from the AZ and going outward through the three regions. First, we examined the number of docked SVs (0–45 nm from AZ) in the two genotypes by EM and showed that they were largely unaltered αβγ-Syn−/− synapses (Figure 2F). Similarly, by cryo-ET, the SV distribution traces showed the characteristic proximal peak (related to docked SVs in EM), indicating that synapses do not suffer from serious release defects. The number of proximal SVs per AZ area (wild-type = 99.58 ± 18.43, αβγ-Syn−/− = 100.81 ± 17.3 per 1 μm^2) and the minimum distance of proximal SVs to the AZ (wild-type = 9.95 ± 0.65 nm, αβγ-Syn−/− = 9.29 ± 0.54 nm) were the same in both genotypes.

Cryo-ET has been used to detect and visualize tethers, protein components that link SVs to the AZ, because these delicate structures are preserved during vitrification but not in conventional EM glutaraldehyde fixation (Figure 3) (Fernández-Busnadiego et al., 2010, 2011). We examined tethering of proximal SVs (<45 nm from AZ) in wild-type and αβγ-Syn−/− synaptosomes by cryo-ET, following procedures we have established (Fernández-Busnadiego et al., 2010, 2011, 2013). Tomographic slices and 3D renderings of tethers and vesicles are shown in Figures 3C and 3D. In wild-type synapses, we found that 55% ± 8.4% of proximal SVs were tethered (have at least one tether), similar to our previously published results (Figure 3E) (Fernández-Busnadiego et al., 2010), while in synapses lacking endogenous synucleins, 80% ± 8.1% of proximal vesicles were tethered (Figure 3E). The number of tethers per proximal SVs was determined and found to be 1.04 ± 0.19 in wild-type synapses and 2.43 ± 0.23 in αβγ-Syn−/− synapses ($p < 0.001$) (Figure 3F). When the length of the tethers was measured, the increase in tethering in αβγ-Syn−/− synapses was largely accounted by short tethers (<5 nm) (Figures 3F, 3H, and 3I). Our

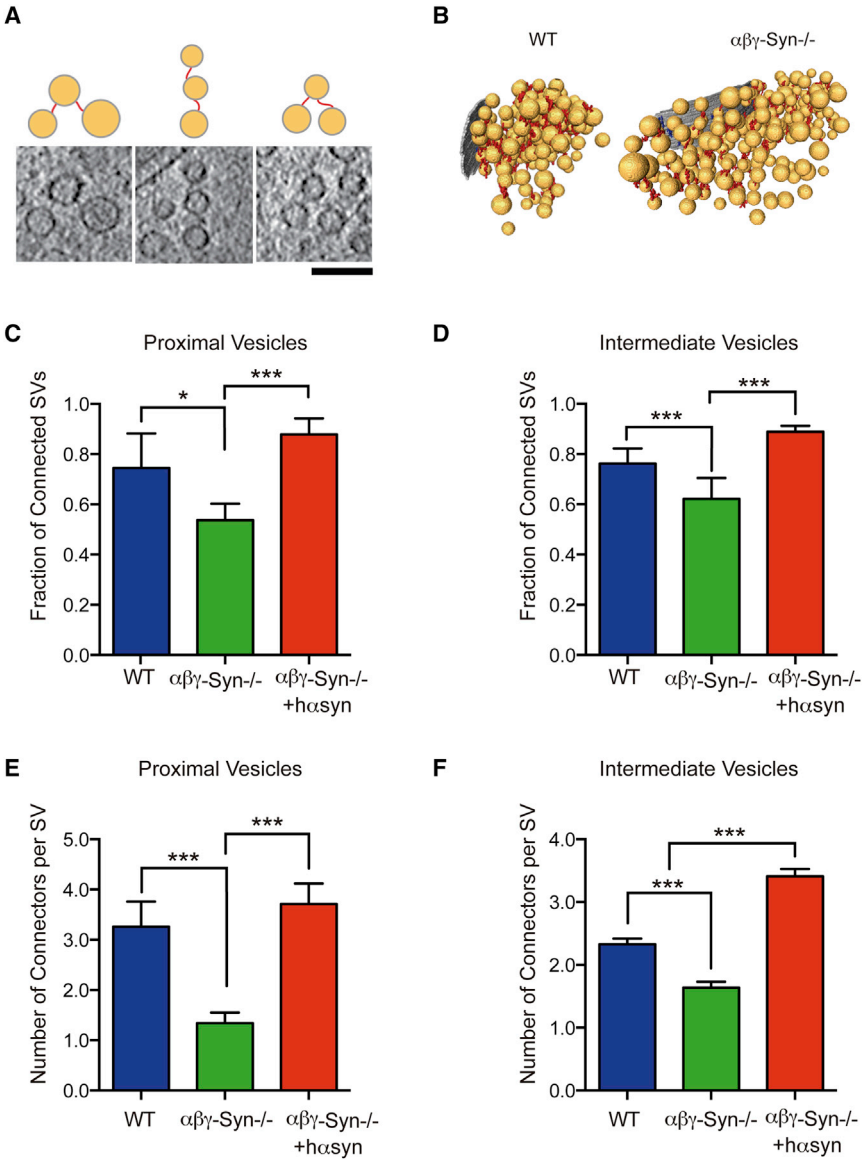

Figure 4. Decreased Connectivity of SVs in αβγ-Syn−/−

(A) Examples of connectors imaged by cryo-ET and corresponding line diagrams. Computationally extracted tomographic, 2-nm-thick slices. Scale bar, 100 nm.

(B) 3D visualization of connectors in wild-type and αβγ-Syn−/− samples by cryo-ET.

(C) Fraction of proximal SVs that have at least one connector in wild-type (blue), αβγ-Syn−/− (green), and synuclein nulls rescued by human α-Syn expression (red).

(D) Fraction of intermediate SVs that have at least one connector in wild-type, αβγ-Syn−/−, and rescued synapses; $p < 0.05$ and $p < 0.001$, respectively, by χ^2 test.

(E) Mean number of connectors per proximal SV in the three genotypes.

(F) Mean number of connectors per intermediate SV in synapses of the three genotypes; $p < 0.001$ for both zones by χ^2 test.

All data are presented as mean ± SEM. n = 3 independent experiments. NS, not significant. $^{**}p < 0.01$, $^{***}p < 0.001$.

and αβγ-Syn−/− synapses (Figures 4A and 4B). In both the proximal and the intermediate zones, the fraction of connected SVs (Figures 4C and 4D) and the number of connectors per SV (Figures 4E and 4F) were decreased in αβγ-Syn−/− synaptosomes. Significantly, we could revert the loss of connectivity by expressing human α-synuclein in the αβγ-Syn−/− background (Figure 4). Specifically, both the fraction of connected SVs and the number of connectors per SV were rescued to wild-type levels by expression of human α-synuclein (Figure 4). Because connectors were still detected in αβγ-Syn−/− synaptosomes by cryo-ET, synucleins are unlikely to be uniquely required for the formation of connectors. However, our findings indicate that synucleins regulate connectors, leading to altered SV connectivity.

previous work has established that proximal SVs in synaptosomes treated with hypertonic sucrose have fewer and longer tethers, leading to the proposal that SVs that have three or more tethers are termed the structurally defined RRP (Fernández-Busnadiego et al., 2010). Therefore, we calculated the fraction of multiply tethered proximal SVs to determine the structurally defined RRP. We found that the fraction of proximal vesicles that belong to structural RRP was increased ~3- to 4-fold in αβγ-Syn−/− synapses compared to the wild-type (WT = 0.149, αβγ-Syn−/− = 0.403; $p < 0.01$) (Figure 3G). These results show that neurons lacking mouse synucleins have a larger structurally defined RRP.

Next, we examined by cryo-ET connectors that interlink SVs located within 250 nm of the AZ. We analyzed the fraction of connected SVs and the number of connectors per SV for proximal (<45 nm) and intermediate (45–250 nm) SVs in wild-type

Finally, we examined by EM the distal vesicles (>250 nm from the AZ) in wild-type and αβγ-Syn−/− synapses. We observe a striking increase in the frequency of clustered SVs in αβγ-Syn−/− synapses. Typical examples of this phenotype are shown in Figures 2B and 5A. We confirmed that these vesicles belong to the reserve pool, as they can be dispersed upon strong stimulation (Figure 5B). This phenotype is also seen in vivo in both the CA1 and the CA3 regions of the hippocampus (Figures 5C and 5D). These experiments show that deletion of synuclein leads to clustering of distal pool vesicles >250 nm from the AZ both in vitro and in vivo. This would suggest that mobilization of reserve pool SVs is different in αβγ-Syn−/− despite similar numbers of SVs to wild-type (Figure 2D). Due to the 250 nm

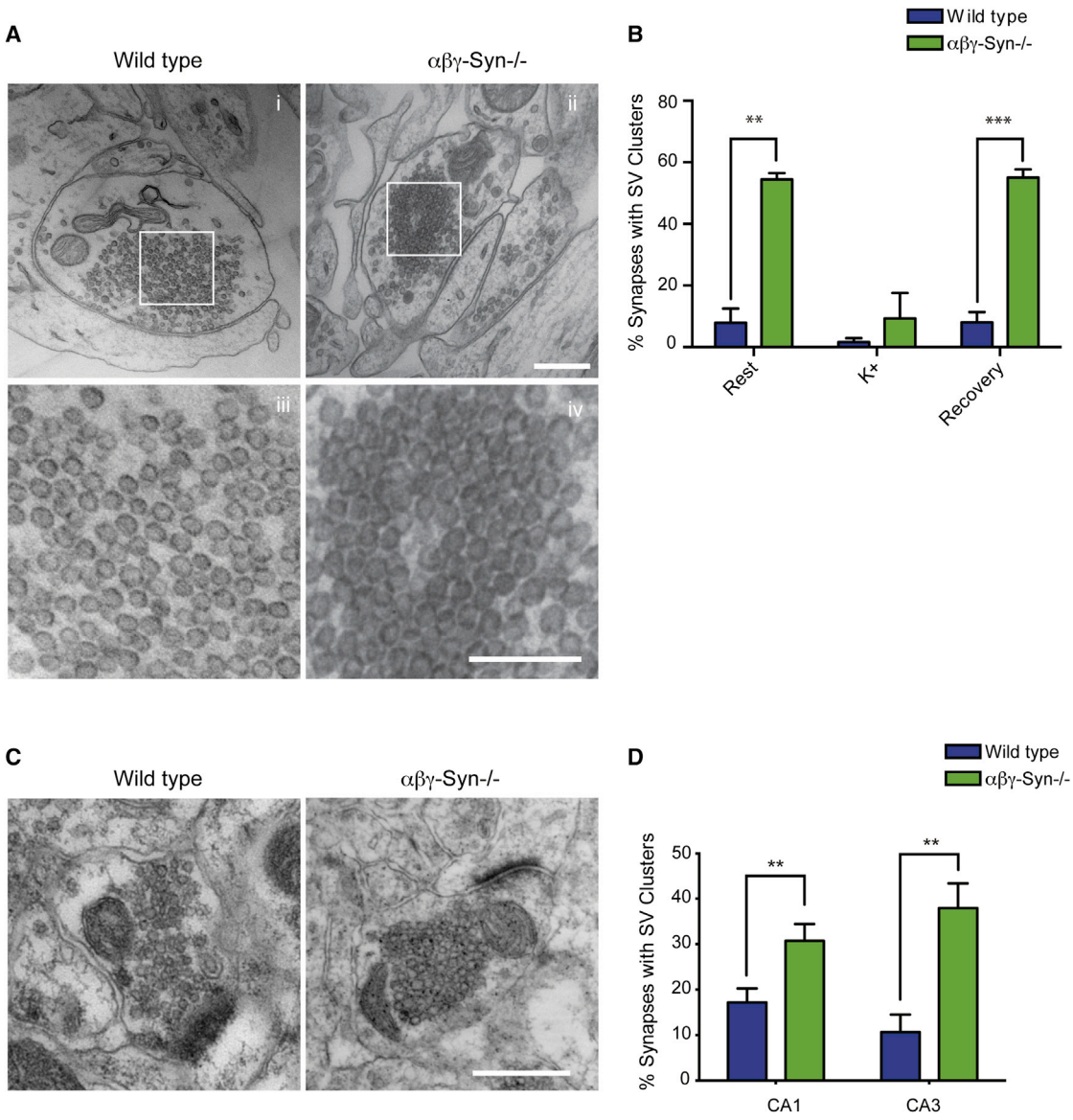

Figure 5. Distal SV Clusters in αβγ-Syn−/− Synapses

(A) Representative micrographs of dissociated hippocampal neurons showing distal SV clusters are present in αβγ-Syn−/− synapses compared to wild-type. (iii–iv) Zoomed-in regions from (i) and (ii), respectively, showing distal vesicles. SVs are clustered and arrayed touching one another in αβγ-Syn−/− synapse.

(B) Quantification of the percentage of synapses with SV clusters in wild-type (blue) and αβγ-Syn−/− (green) neurons at rest, after 90 s of stimulation with 45 mM K^+ and subsequent recovery for 10 min. SV clusters disperse upon high K^+ stimulation. n = 3 independent neuronal cultures; 50–150 synapses per genotype per culture were analyzed.

(C) Micrographs of CA1 synapses from wild-type and αβγ-Syn−/− mice.

(D) Quantification of synapses with SV clusters in CA1 and CA3 regions of the brain. n = 2–3 mice/genotype.

All data are presented as mean ± SEM. Scale bar, 400 nm; scale bar for (Aiii) and (Aiv), 200 nm. **p < 0.01, ***p < 0.001.

imposed cryo-ET limit, we were unable to determine whether the increased distal SV clustering in αβγ-Syn−/− (Figures 2B and 5) is due to altered connectivity.

Biochemical Changes in Synuclein Null Synapses: Clues to SV Pool Organization

To be able to ascribe the ultrastructural changes in αβγ-Syn−/− synapses to molecular changes, we need to catalog the proteomic changes induced by the absence of synucleins. We have previously systematically compared the entire synaptic proteome of wild-type and αβγ-Syn−/− brains, allowing us to begin to make such ultrastructural-molecular associations. αβγ-Syn−/− synapses showed select changes (Greten-Harrison et al., 2010; Westphal and Chandra, 2013; Vargas et al., 2014; Burré et al., 2010). The upregulated proteins (Endophilin A1 and A2, Synapsin IIb, and Annexin V) and downregulated

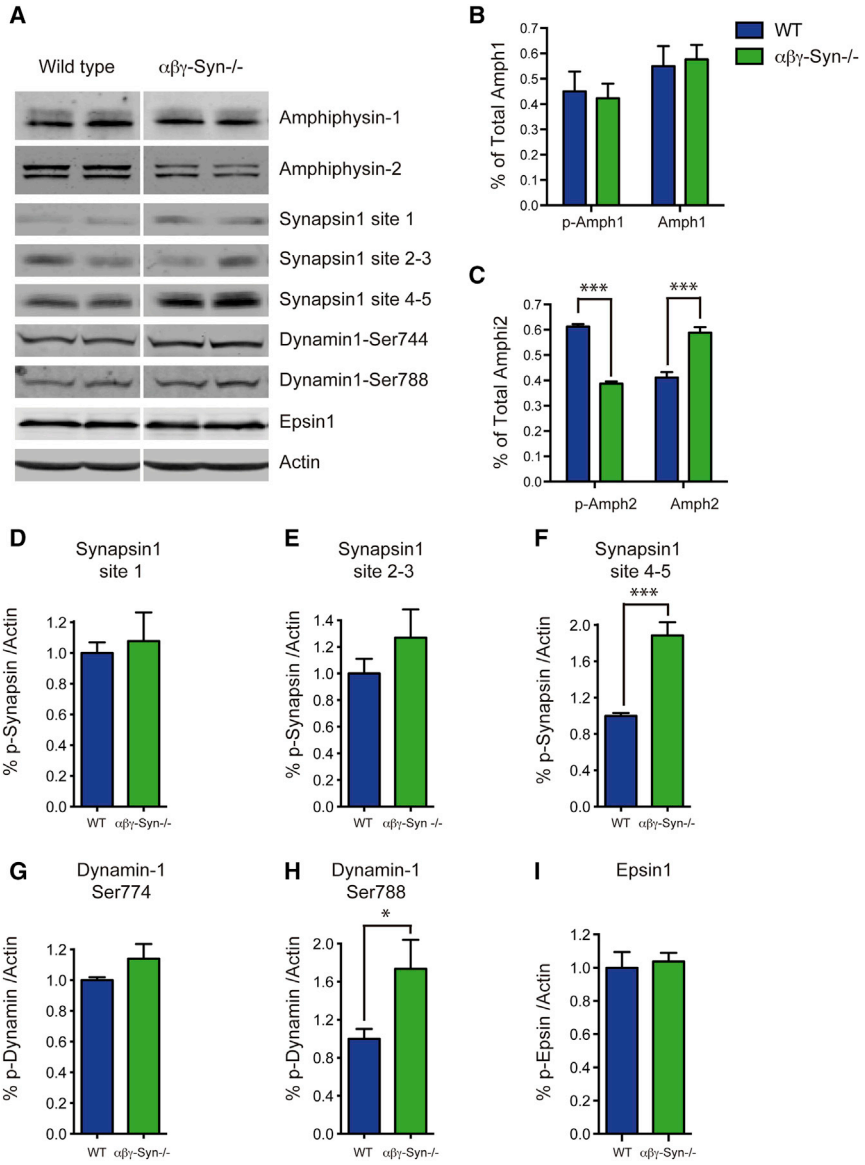

Figure 6. Biochemical Changes in αβγ-Syn−/− in Candidate Proteins that Regulate SV Connectivity

(A) Representative western blots of wild-type and αβγ-Syn−/− synaptosomes for the denoted proteins.

(B) Quantification of levels of total and phosphorylated (top band) amphiphysin-1.

(C) Quantification of phospho- (top band) and dephospho-amphiphysin-2 (bottom band) in the two genotypes.

(D–I) Phosphorylation of synapsin I at site 1 (D), site 3 (E), and sites 4 and 5 (F); Dynamin-1 site 774 (G) and site 788 (H); and Epsin-1 (I) in wild-type and αβγ-Syn−/− synaptosomes.

All data are presented as mean ± SEM. n = 3 independent experiments. NS, not significant. *p < 0.05, ***p < 0.001.

proteins (synaptobrevin 2 and AP180) may mediate SV tethering, connectivity, and distal clustering changes seen in αβγ-Syn−/−.

It has been proposed that connectors are peripheral SV proteins that behave differentially upon phosphorylation. Even though the molecular identity of the connectors remains to be determined, several candidates have been put forward based on these properties (Table S1). We analyzed the phosphorylation of the most prominent candidates in wild-type and αβγ-Syn−/− synaptosomes by immunoblotting with phospho-site-specific antibodies. Synapsins, which are known to regulate reserve pool SVs via their phosphorylation status (Rosahl et al., 1995; Gaffield and Betz, 2007; Benfenati et al., 1993), were proposed to interlink SVs (Hirokawa et al., 1989). Synapsin I sites 1, 2, and 3 were unchanged in comparing wild-type and αβγ-Syn−/− (Figures 6A, 6D, and 6E). However, the baseline phosphorylation of synapsin I at sites 4 and 5 was increased (148%) (Figures 6A and 6F). Next, we tested other candidate proteins implicated in SV pool regulation, namely, amphiphysins, epsins, and dynamin (Chen et al., 1999; Clayton et al., 2010). We observed changes in amphiphysin-2, with a greater percentage of dephosphorylated amphiphysin-2 present in αβγ-Syn−/− samples. In contrast, there was no change in the level of phospho-amphiphysin-1 (Figures 6A and 6B). There were no changes in phosphorylation of epsin-1 or dynamin-1 at position 774 (Figures 6G–6I), but we did observe an increase in dynamin-1 phosphorylation at position 778. Because phosphorylation of synapsin I at sites 4 and 5, amphiphysin 2, and dynamin-1 at position 778 are regulated by the phosphatase calcineurin (Table S1), we tested the effect of its inhibitor Cyclosporin A. As expected, the drug increases phosphorylation of these proteins, thus ameliorating the decreased phosphorylation of amphiphysin-2 in αβγ-Syn−/− and further increasing phosphorylation of synapsin I at sites 4 and 5 and dynamin-1 at position 778 (Figure S1). Collectively, the pattern of phosphorylation events that occurs upon deletion of synucleins is known to promote SV endocytosis but may contribute to alter SV clustering and decreased connectivity as well.

Previous studies have established that strong stimulation of synapses leads to phosphorylation changes (Table S1) and dispersion of the reserve pool SVs. To test whether this is also the case in αβγ-Syn−/−, we strongly stimulated synaptosomes to disperse SV clusters as in Figure 5B and monitored the changes in phosphorylation of amphiphysin-2 and synapsin sites 4 and 5. As anticipated, we could dephosphorylate amphiphysin-2 and synapsin I with high K^+, though the magnitude of the changes was different in the two genotypes (Figure S2), indicating that these two processes are correlated.

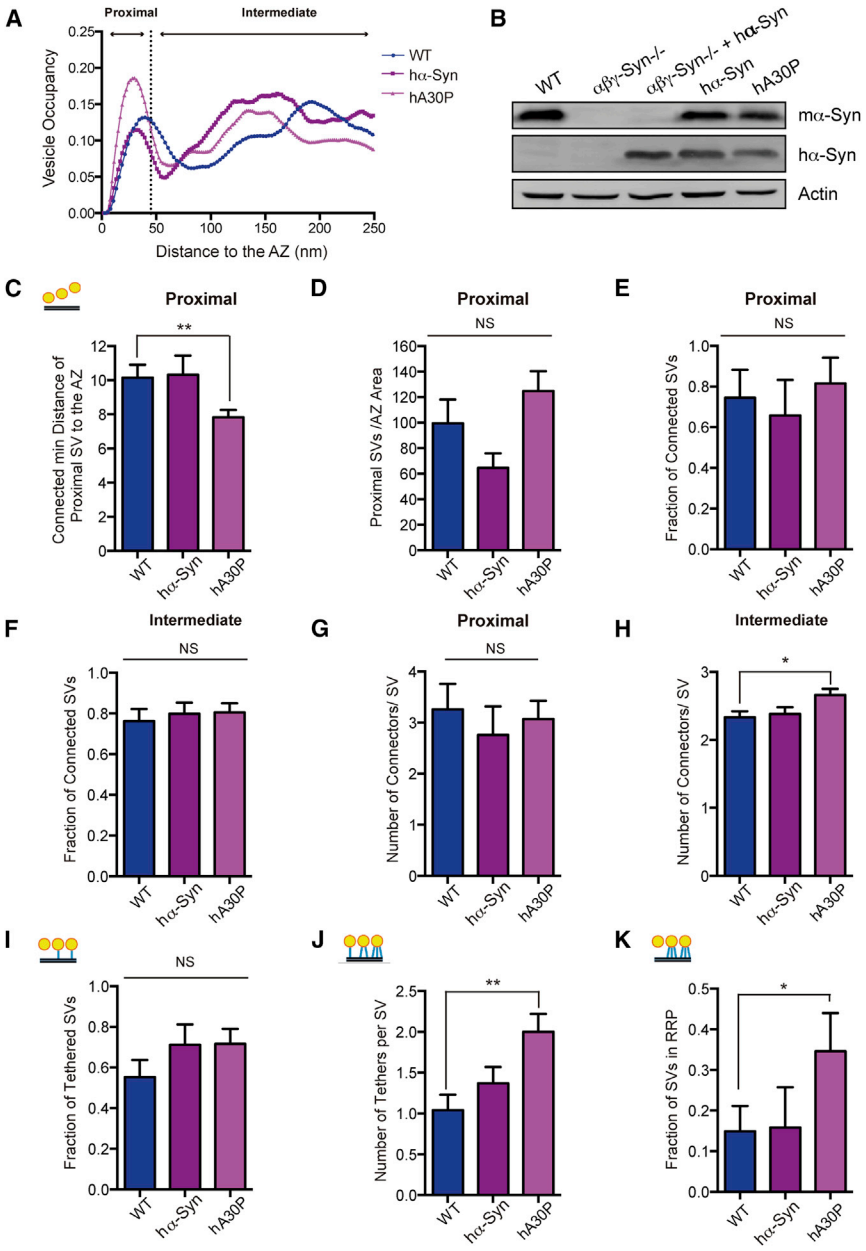

Figure 7. α-Synuclein PD Mutants Primarily Alter Tethering

(A) SV distribution calculated as the fraction of cytoplasmic volume occupied by SVs in the first 250 nm from the AZ of wild-type (WT; blue), human α-synuclein overexpressing (hα-Syn; purple), and human A30P (hA30P) mutant α-synuclein (mauve) overexpressing transgenics.

(B) Western blotting of synaptosomes of the denoted genotypes. m = mouse, h = human.

(C) Mean distance of proximal SVs to the AZ, in which the distance between a SV and the AZ is calculated as the minimal distance between them. $p < 0.05$ by t test.

(D) Mean number of proximal SVs per AZ area in wild-type, hα-Syn, and hA30P.

(E) Fraction of proximal SVs that have at least one connector in WT, hα-Syn, and hA30P overexpressing transgenic synapses.

(F) Fraction of intermediate SVs that have at least one connector in wild-type, hα-Syn, and hA30P synapses.

(G) Mean number of connectors per proximal SV in the three genotypes.

(H) Mean number of connectors per intermediate SV in the three genotypes.

(I) Fraction of proximal SVs that have at least one tether in wild-type, hα-Syn, and hA30P.

(J) Mean number of tethers per proximal SV in the three genotypes.

(K) Number of proximal SVs with two or more greater tethers (structural RRP). $p < 0.01$ by K-W test and $p < 0.05$ by χ^2 test, respectively.

All data are presented as mean ± SEM. n = 3 independent experiments. NS, not significant. *p < 0.05, **p < 0.01, ***p < 0.001.

Effect of Familial PD Mutations on Presynaptic Structure

Several EM studies have examined the overexpression of human α-synuclein and consistently show an enlargement of presynaptic termini all the way to hypertrophy, as well as a greater dispersion of reserve pool SVs (Boassa et al., 2013; Nemani et al., 2010; Scott et al., 2010; Busch et al., 2014). To further investigate how PD mutants affect synapse structure, we focused on how PD mutants influence the presynaptic cytomatrix. We previously developed and characterized transgenic human α-synuclein mice that either carry the A30P mutation, like a subset of PARK1 patients, or overexpress wild-type human α-synuclein, like PARK4 patients (Chandra et al., 2005; Gallardo et al., 2008). These transgenic mice have ~5-fold α-synuclein in the brain compared to wild-type mice, consistent with published data (Figure 7B) (Chandra et al., 2005). The α-synuclein transgenics develop age-dependent PD-like phenotypes, accompanied by α-synuclein aggregation and neuronal loss (Chandra et al., 2005; Gallardo et al., 2008).

Cryo-ET data showed that the distribution of SVs was normal in synaptosomes of PD mutant (PARK1/hA30P and PARK4/hα-syn) mice (Figure 7A), though there were 35% fewer proximal vesicles per AZ area in PARK4/hα-syn and 25% more in PARK1/hA30P synaptosomes (not significant [n.s.]) (Figures 7A and 7D). The mean distance of proximal SVs to the AZ was significantly reduced in the PARK1/hA30P mutant with respect to the wild-type ($p < 0.05$). This distance was further reduced when only the connected proximal SVs were considered ($p < 0.01$), while there was no significant difference for any other genotypes (Figure 7C).

We then examined both tethers (Figures 7I–7K) and connectors (Figures 7D–7H) in wild-type and α-synuclein transgenic synaptosomes. The fraction of proximal SVs that were tethered was not significantly changed (Figure 7I), but the number of

tethers per proximal SV (Figure 7J), as well as the fraction of proximal vesicles with multiple tethers, i.e., structurally defined RRP, were all significantly increased in PARK1/hA30P α-synuclein transgenic compared to wild-type samples ($p < 0.01$ by Kruskal-Wallis [K-W] test and $p < 0.05$ by χ^2 test, respectively) (Figure 7K), while there were no significant changes in PARK4/hα-syn synapses. The increased tethering (Figures 7I–7K) and decreased mean distance of connected proximal SVs to AZ (Figure 7D) suggest that PARK1/hA30P synapses have specific structural alterations in the proximal zone, which may be related to neurotransmitter release alterations.

The inverse correlation between the mean number of tethers per proximal SV and the vesicle distance to the AZ, a sensitive indicator of synaptic release (Fernández-Busnadiego et al., 2013), was present in wild-type and PARK1/hA30P but absent in PARK4/hα-syn synapses (Table S2). Taking into account that tethering was not altered, our data suggest that PARK4 synapses show a mild release deficit. This finding is consistent with published electrophysiological studies that show overexpression of human wild-type α-synuclein decreases neurotransmission (Nemani et al., 2010; Janezic et al., 2013; Scott and Roy, 2012).

Regarding SV connectivity, there was only a modest increase in the mean number of connectors per SV in PARK1/hA30P synaptosomes (Figures 7E–7H). The connectivity of the proximal SVs showed a significant dependence on the interaction between the human α-synuclein expression and the level of endogenous synucleins ($p < 0.05$, factorial design ANOVA). These data, along with those for αβγ-Syn−/− synapses (Figure 5), indicate that the SV interconnectivity is primarily sensitive to the loss of synucleins. To determine the phosphorylation changes associated with PARK1/hA30P and PARK4/hα-syn synapses, we immunoblotted for the three phosphoproteins changed in αβγ-Syn−/− synapses. We find the phosphorylation of amphiphysin-2 in PARK1/hA30P and PARK4/hα-syn synapses is similar to wild-type, while the phosphorylation status of synapsin I sites 4 and 5 is decreased in PARK4/hα-syn only (Figures S3A and S3B). Dynamin-1 position 778 phosphorylation is increased in both PD mutants relative to wild-type (Figure S3C).

Collectively, these observations indicate there are select disturbances in SV tethering and connectivity depending on the α-synuclein PD mutation.

DISCUSSION

In this study, we systematically investigated the impact of deleting synucleins and expressing PD mutants of α-synuclein on synapse architecture. We find multiple effects of synucleins on presynaptic termini, consistent with the fact that they are abundantly expressed and have conformational plasticity.

Synucleins Are Important Determinants of Synapse Size

We observed smaller synapses in αβγ-Syn−/− cultured neurons (Figure 2D), a phenotype first seen in synuclein null brain sections (Greten-Harrison et al., 2010). Several groups have reported that overexpression of wild-type human α-synuclein leads to increased synapse size, suggesting that synucleins can bidirectionally control synapse size. The linear relationship between synuclein levels and synaptic size also indicates that synucleins are influencing insertion and removal of membrane. This is in line with ascribed functions of synucleins in SV exo- and endocytosis (Burré et al., 2010; Vargas et al., 2014; Busch et al., 2014), although the precise relationship between synapse size and trafficking is unknown.

αβγ-Syn−/− Synapses Have Increased Short Tethers in the Proximal Zone

Our cryo-ET results showed that wild-type and αβγ-Syn−/− synapses have similar number and distribution of SVs, arguing against major disturbances in the synaptic release. However, we observe a robust increase in the SV tethering, as well as the fraction of SVs in structurally defined RRP pool in αβγ-Syn−/− synapses (Figures 3C–3I). Tethers are hypothesized to be soluble NSF attachment protein receptors (SNAREs) or constituents of AZ such as Rim 1, based on their lengths and tetanus toxin susceptibility. By our analysis of αβγ-Syn−/− synapses, we can clearly establish that synucleins are not tethers but that endogenous synucleins negatively regulate short tethers. This is possibly because deletion of synucleins stabilizes certain SNARE assemblies on the synaptic membrane, perhaps due to the absence of the α-synuclein-synaptobrevin 2 interaction (Burré et al., 2010) or decreased levels of AP180, the endocytic adaptor for synaptobrevin 2 (Koo et al., 2015) in αβγ-Syn−/− synapses (Vargas et al., 2014). The number of docked SVs and their distribution in the proximal zone were unaltered (Figures 2F and 3B) but the structural RRP was increased in αβγ-Syn−/− synapses (Figure 3G), which suggests a larger number of docked SVs are primed. This interpretation is consistent with our previous work characterizing the electrophysiology of αβγ-Syn−/− showing increased basal transmission (Greten-Harrison et al., 2010). However, this proposition is not in line with the finding that the number of SNARE complexes is reduced in αβγ-Syn−/− brain homogenate (Burré et al., 2010); we did not find the number of SNAREs is reduced in the brain homogenates of young αβγ-Syn−/− (Greten-Harrison et al., 2010; unpublished data). Regardless, the increased tethers in αβγ-Syn−/− synapses could mean that the number of short tethers are not directly proportional to the number of SNARE complexes in the brain. In keeping with this idea, Imig et al. (2014) have suggested that SV docking is mediated by Munc13. With our result that synucleins negatively regulate short tethers, future studies can begin to investigate the exact nature of SNARE machinery that may constitute short tethers.

SV Connectivity within 250 nm of the AZ and Characteristics of Connectors

Deletion of endogenous synucleins caused a decrease in SV connectivity, which was rescued upon human α-synuclein overexpression (Figures 4C–4F), suggesting that both mouse and human synucleins support SV connectivity. On the surface, this loss of connectivity appears at odds with our EM data showing increased clustering (>250 nm) in αβγ-Syn−/− (Figure 5). However, the connectivity decrease was detected at closer distances to the AZ (<250 nm), suggesting that there are distinct connectors for regions of the presynaptic terminal. Furthermore, our data agree with the observation that α-synuclein clusters SVs in reconstituted systems (Diao et al., 2013) and suggest that

the increase in connectivity is a structural correlate of the synuclein-dependent increase in clustering and decrease of SV trafficking *in vitro* (Wang et al., 2014).

The molecular constituents of connectors in the 0–250 nm zone are not yet established. Our previous cryo-ET studies had revealed that these connectors are dynamic structures that respond to phosphorylation. Because we observed phosphorylation changes in synapsin 1, amphiphysin-2, and dynamin-1 in αβγ-Syn−/−, we can categorize these proteins as potential connectors. It was proposed that synapsins mediate SV connectivity, but analysis suggests that other proteins are involved (Benfenati et al., 1993; Hirokawa et al., 1989; Gaffield and Betz, 2007; Siksou et al., 2007, 2011). Our finding that synapsin I site 4 and 5 phosphorylation is decreased in PARK4/hα-syn but connectivity was unchanged in this genotype also suggests proteins other than synapsin I may form connectors. The levels of phosphorylated amphiphysin-2 are in line with the changes we observe in connectors, raising the possibility that phospho-amphiphysin-2 makes up or regulates connectors (Table S3). The finding that the phosphatase calcineurin dephosphorylates these proteins (Figure S1) strongly implies it is a key player in the regulation of connectors.

Distal SV Organization

Using EM, the most striking phenotype we observe in αβγ-Syn−/− synapses is that distal SVs are clustered (Figures 2 and 5). SV density is higher; it is possible that the SVs are clustered together because the volume of each synapse is smaller. However, this is not a likely explanation, because we often find clustered SVs even in areas devoid of larger structures that could constrain the SVs (Figure 5). This complements an earlier EM result showing that overexpression of α-synuclein disperses reserve pool SVs (Nemani et al., 2010), hinting at a bidirectional effect of synapse structure by synuclein levels.

Biochemically, we observed changes in phosphorylation of synapsin 1 (sites 4 and 5), amphiphysin-2, and dynamin-1 in αβγ-Syn−/− synapses (Figure 6). The changes in synapsin sites 4 and 5 have been hypothesized to control synaptic vesicle endocytosis (Cesca et al., 2010), similar to other endocytic proteins that are dephosphorylated upon stimulation, the so-called dephosphins (dynamin-1, epsin-1, and amphiphysin). Collectively, the changes in phosphorylation of peripheral SV proteins in αβγ-Syn−/− (Figure 6) could compensate for the endocytic regulation that synucleins normally exert (Vargas et al., 2014). This conclusion is strengthened by the previously reported upregulation of Synapsin IIb (Westphal and Chandra, 2013), the isoform that lacks phosphorylation sites 2 and 3 but contains sites 4 and 5. But more intriguingly, these results open the possibility that these proteins also regulate distal SV connectors to control SV clustering and mobility.

PARK1 and PARK4 Mutants: How Do They Influence Synaptic Structure and Function?

Structurally, the PARK mutants were not the opposite of the synuclein nulls, even though some phenotypes, such as synapse size and distal SV clustering, are reversed in these two set of mice. The PARK1 and PARK4 mutants have distinct phenotypes that set them apart from wild-type mice.

The PARK1/hA30P mutant shows increased tethering (Figures 7J and 7K) that mirrors that in αβγ-Syn−/− synapses (Figure 3). This is consistent with previous predictions that the A30P mutant is both a loss-of-function mutation and a gain-of-function mutation (Chandra et al., 2005). The loss of function is likely because the PARK1/hA30P mutant does not fold completely in the presence of acidic lipids and is targeted inefficiently to synapses. Functionally, the A30P mutant is associated with decreased neurotransmitter release in only some types of dopaminergic synapses (Taylor et al., 2014) and not in hippocampal synapses (Nemani et al., 2010), quite different from the αβγ-Syn−/− synapses. These differences might be due to the increased connectivity of SVs in the intermediate zone of PARK1/hA30P and the decreased connectivity in αβγ-Syn−/− transgenic synapses (Figure 7H).

In contrast to PARK1/hA30P, the PARK4/hα-syn mutation had no significant effect on tethering. Yet the absence of the inverse correlation between the mean number of tethers per proximal SV and the vesicle distance to the AZ (Table S2) indicates that PARK4 synapses show a mild release-related structural deficit. This is consistent with the work from many groups that showed that overexpression of human wild-type α-synuclein leads to decreased neurotransmission (Nemani et al., 2010; Janezic et al., 2013; Taylor et al., 2014; Wang et al., 2014; Scott and Roy, 2012). Our data indicate that this effect has a structural basis.

Compared to tethering, we find few effects from both PD mutations on connectors and proximal intermediate SV interconnectivity. However, decreased reserve pool SV clustering has been previously seen by EM (Nemani et al., 2010; Scott et al., 2010). This again suggests that the nature of connectors varies within the presynaptic terminal.

Significantly, structural changes in the presynaptic cytomatrix are already observed in synaptic samples derived from 3-month-old PARK1/hA30P and PARK4/hα-syn mice, suggesting that with increasing age, it may lead to more pronounced synaptic dysfunction and eventually synapse loss seen in PD. Overall, our data point to synucleins as a major orchestrator of presynaptic structure.

EXPERIMENTAL PROCEDURES

Animals

αβγ-Syn−/− mice, as well as human wild-type and A30P α-synuclein transgenics, have been previously described (Chandra et al., 2005; Greten-Harrison et al., 2010). The mice are maintained under the aegis of an approved Institutional Animal Care and Use Committee (IACUC) protocol.

Antibodies

α-Synuclein antibody was purchased from BD Biosciences, amphiphysin-1 and amphiphysin-2 (bin1) were purchased from Upstate, and synapsin antibodies were a gift from Dr. Angus Nairn, Yale University. Synapsin I sites 4 and 5 and Dynamin-1 Ser-774 were purchased from Phosphosolutions, and Epsin antibody was provided by Dr. Pietro De Camilli, Yale University.

Synaptosome Preparation

Synaptosomes are an established model for neurotransmitter release that can sustain multiple exocytic cycles and are susceptible to pharmacological manipulations (Nicholls and Sihra, 1986; Whittaker, 1993; Nicholls, 2003). Synaptosomes were prepared from 2- to 3-month-old mice as described (Dunkley

et al., 1988; Godino et al., 2007). Brains from mice of the denoted genotypes were homogenized in sucrose buffer (2 mM HEPES [pH 7.4], 320 mM sucrose, 5 mM EDTA, 2 mM DTT). The homogenates were centrifuged at 3,000 g for 2 min. The supernatant (S1) was centrifuged twice at 9,200 g for 15 min to obtain a crude synaptosomal fraction (P3). The P3 fraction was separated on a Percoll gradient (3%, 10%, and 23%) by centrifugation (18,700 g × 12 min). The synaptosomes were taken from the interface between the 10% and the 23% layers, washed, and pelleted using modified Tyrode's buffer (140 mM NaCl, 5 mM KCl, 5 mM NaHCO3, 1.2 mM NaHPO4, 1 mM $MgCl_2$, 10 mM glucose, 10 mM HEPES [pH 7.4]).

Immuno-EM

Purified synaptosomes (n = 46 images from three WT mice and 25 images from two knockout [KO] mice) were fixed using a hypotonic fixative (3% paraformaldehyde and 0.25% glutaraldehyde in 5 mM phosphate buffer [pH 7.4]). Because of the hypotonic fixation step, we primarily see membrane-associated proteins in this procedure. The sample was embedded in gelatin, solidified, and cut in little cubes. The cubes were incubated with primary and secondary antibodies in incubation buffer (5% BSA, 0.5 M NaCl, 0.02 M phosphate buffer). Samples were then dehydrated, embedded in Epon, and sectioned. Uranyl acetate staining was performed, and then samples were imaged using a Phillip CM10 transmission electron microscope. The resulting electron micrographs were analyzed for the distribution of gold particles. Gold articles within 9 nm of a vesicle, membrane, or mitochondria were assigned to these categories, while the remaining particles were assigned to the cytosol.

Conventional EM of Neuronal Cultures

Primary hippocampal neurons grown on coverslips were incubated in Tyrode's buffer for 5 min. Subsequently, the coverslips were (1) fixed immediately, (2) stimulated for 2 min by adding high K^+ Tyrode's buffer (45 mM KCl) before fixing, or (3) allowed to recover poststimulation in Tyrode's buffer for 10 min before fixing. All incubations were done at 37°C. Fixation was performed for 1 hr with 1.2% glutaraldehyde in 66 mM sodium cacodylate. Postfixation was done for 1 hr in 1% OsO_4 and 1% $KFe(CN)_6$-0.1 M sodium cacodylate. Neurons were stained overnight with 2% uranyl magnesium acetate, dehydrated in increasing ethanol concentrations, and embedded in Epon. Samples were processed for imaging by standard procedures. Pictures were captured using a Phillip CM10 transmission electron microscope. Synapses (50–150) were analyzed for each condition and repeated using three independent cultures.

Morphometric analysis was done on glutamergic synapses as described in Greten-Harrison et al. (2010). Analysis was blind to genotype. We defined distal SV clusters as 20 or more SVs in physical contact with one another and arrayed.

Cryo-ET

Vitrification of synaptosomes, tomographic acquisition, and analysis were done as described previously (Fernández-Busnadiego et al., 2010). Briefly, a 3 μL drop of 10 nm colloidal gold (Sigma-Aldrich) was deposited on plasma-cleaned holey carbon copper EM grids (Quantifoil) and allowed to dry. A 3 μL drop of synaptosomal suspension was placed onto the grid, blotted with filter paper (GE Healthcare), and plunged into liquid ethane. Vitrified grids were stored in liquid nitrogen.

Vitrified synaptosomes were imaged on a FEI Tecnai G2 Polara microscope equipped with an field emission gun (FEG) operated at 300 keV and a postcolumn energy filter (Gatan) operating in zero-loss mode. Images were recorded on a Gatan MegaScan charge-coupled device (CCD) camera at a pixel size at the specimen level of 0.47–0.57 nm at 6 μm underfocus. Tilt series were acquired at 1.5°–2° angular increments, typically from −60° to +60°, using the FEI tomography software. Between six and nine tomograms were processed for each condition. Tomograms were aligned using gold beads as fiducial markers, binned twice (final pixel size, 1.9–2.3 nm), and reconstructed using IMOD and TOM packages (Kremer et al., 1996; Nickell et al., 2005). An analytical weighted back-projection (WBP) algorithm was used for reconstruction.

Tomograms were slightly denoised using anisotropic nonlinear diffusion (Frangakis and Hegerl, 2001; Fernández and Li, 2003). SVs and the AZ membrane were manually segmented in Amira software (FEI). Tethers and connectors were automatically segmented (using hierarchical connectivity segmentation) and analyzed using Pyto software (Lučić et al., 2016; available on demand) as previously described (Fernández-Busnadiego et al., 2013). Tether lengths were estimated from the positions of voxels that contact the vesicle membrane or the AZ. Consequently, connector and tether lengths calculated membrane to membrane would be approximately 1 pixel longer.

The numbers of mice, synapses, SVs, proximal SVs, tethers, and connectors analyzed are included in Table S4.

Data Analysis

All data are presented as mean ± SEM. Statistical tests used are indicated in figure legends. Means and SEM were calculated over all measurements of a specific property. We used the K-W test (nonparametric) for values deviating from the normal distribution (e.g., number of tethers or connectors per vesicle). When values fell into discrete bins (e.g., fraction of connected and nonconnected vesicles), the χ^2 test was used and the SEM was calculated between synapses. We used Pearson's coefficient for correlation analysis, and its significance was determined using the t test. In all cases, confidence levels were calculated using two-tailed tests.

SUPPLEMENTAL INFORMATION

Supplemental Information includes three figures and four tables and can be found with this article online at http://dx.doi.org/10.1016/j.celrep.2016.12.023.

AUTHOR CONTRIBUTIONS

K.J.V., N.S., T.D., R.F.-B., Y.V.T., and U.L. performed experiments and analyzed data. S.S.C. and V.L. analyzed data. S.S.C., V.L., and K.J.V. wrote the paper. All authors edited the text.

ACKNOWLEDGMENTS

We thank Pietro De Camilli for advice and for providing reagents and Wolfgang Baumeister for providing access to cryo-ET instrumentation. We also thank our colleagues Mirko Messa and Christopher Westphal for help with biochemistry and Andrew Williams, Yumei Wu, and Summer Paradise for help with EM. This work was supported by NIH grants R01NS083846 and R01NS064963 and a Bumpus Foundation grant (to S.S.C.). R.F.-B. is the recipient of a Feodor Lynen postdoctoral fellowship from the Humboldt Foundation. K.J.V. is the recipient of a fellowship from the Pew Foundation.

Received: August 5, 2016
Revised: October 21, 2016
Accepted: December 7, 2016
Published: January 3, 2017

REFERENCES

Altrock, W.D., tom Dieck, S., Sokolov, M., Meyer, A.C., Sigler, A., Brakebusch, C., Fässler, R., Richter, K., Boeckers, T.M., Potschka, H., et al. (2003). Functional inactivation of a fraction of excitatory synapses in mice deficient for the active zone protein bassoon. Neuron *37*, 787–800.

Atasoy, D., Schoch, S., Ho, A., Nadasy, K.A., Liu, X., Zhang, W., Mukherjee, K., Nosyreva, E.D., Fernandez-Chacon, R., Missler, M., et al. (2007). Deletion of CASK in mice is lethal and impairs synaptic function. Proc. Natl. Acad. Sci. USA *104*, 2525–2530.

Bellucci, A., Mercuri, N.B., Venneri, A., Faustini, G., Longhena, F., Pizzi, M., Missale, C., and Spano, P. (2016). Review: Parkinson's disease: from synaptic loss to connectome dysfunction. Neuropathol. Appl. Neurobiol. *42*, 77–94.

Benfenati, F., Valtorta, F., Rossi, M.C., Onofri, F., Sihra, T., and Greengard, P. (1993). Interactions of synapsin I with phospholipids: possible role in synaptic vesicle clustering and in the maintenance of bilayer structures. J. Cell Biol. *123*, 1845–1855.

Boassa, D., Berlanga, M.L., Yang, M.A., Terada, M., Hu, J., Bushong, E.A., Hwang, M., Masliah, E., George, J.M., and Ellisman, M.H. (2013). Mapping the subcellular distribution of α-synuclein in neurons using genetically encoded probes for correlated light and electron microscopy: implications for Parkinson's disease pathogenesis. J. Neurosci. *33*, 2605–2615.

Burré, J., Sharma, M., Tsetsenis, T., Buchman, V., Etherton, M.R., and Südhof, T.C. (2010). Alpha-synuclein promotes SNARE-complex assembly in vivo and in vitro. Science *329*, 1663–1667.

Busch, D.J., Oliphint, P.A., Walsh, R.B., Banks, S.M., Woods, W.S., George, J.M., and Morgan, J.R. (2014). Acute increase of α-synuclein inhibits synaptic vesicle recycling evoked during intense stimulation. Mol. Biol. Cell *25*, 3926–3941.

Calo, L., Wegrzynowicz, M., Santivañez-Perez, J., and Grazia Spillantini, M. (2016). Synaptic failure and α-synuclein. Mov. Disord. *31*, 169–177.

Cesca, F., Baldelli, P., Valtorta, F., and Benfenati, F. (2010). The synapsins: key actors of synapse function and plasticity. Prog. Neurobiol. *91*, 313–348.

Chandra, S., Gallardo, G., Fernández-Chacón, R., Schlüter, O.M., and Südhof, T.C. (2005). Alpha-synuclein cooperates with CSPalpha in preventing neurodegeneration. Cell *123*, 383–396.

Chen, H., Slepnev, V.I., Di Fiore, P.P., and De Camilli, P. (1999). The interaction of epsin and Eps15 with the clathrin adaptor AP-2 is inhibited by mitotic phosphorylation and enhanced by stimulation-dependent dephosphorylation in nerve terminals. J. Biol. Chem. *274*, 3257–3260.

Clayton, D.F., and George, J.M. (1999). Synucleins in synaptic plasticity and neurodegenerative disorders. J. Neurosci. Res. *58*, 120–129.

Clayton, E.L., Sue, N., Smillie, K.J., O'Leary, T., Bache, N., Cheung, G., Cole, A.R., Wyllie, D.J., Sutherland, C., Robinson, P.J., and Cousin, M.A. (2010). Dynamin I phosphorylation by GSK3 controls activity-dependent bulk endocytosis of synaptic vesicles. Nat. Neurosci. *13*, 845–851.

De Camilli, P., Harris, S.M., Jr., Huttner, W.B., and Greengard, P. (1983). Synapsin I (protein I), a nerve terminal-specific phosphoprotein. II. Its specific association with synaptic vesicles demonstrated by immunocytochemistry in agarose-embedded synaptosomes. J. Cell Biol. *96*, 1355–1373.

Diao, J., Burré, J., Vivona, S., Cipriano, D.J., Sharma, M., Kyoung, M., Südhof, T.C., and Brunger, A.T. (2013). Native α-synuclein induces clustering of synaptic-vesicle mimics via binding to phospholipids and synaptobrevin-2/VAMP2. eLife *2*, e00592.

Dunkley, P.R., Heath, J.W., Harrison, S.M., Jarvie, P.E., Glenfield, P.J., and Rostas, J.A. (1988). A rapid Percoll gradient procedure for isolation of synaptosomes directly from an S1 fraction: homogeneity and morphology of subcellular fractions. Brain Res. *441*, 59–71.

Fernández, J.J., and Li, S. (2003). An improved algorithm for anisotropic nonlinear diffusion for denoising cryo-tomograms. J. Struct. Biol. *144*, 152–161.

Fernández-Busnadiego, R., Zuber, B., Maurer, U.E., Cyrklaff, M., Baumeister, W., and Lucic, V. (2010). Quantitative analysis of the native presynaptic cytomatrix by cryoelectron tomography. J. Cell Biol. *188*, 145–156.

Fernández-Busnadiego, R., Schrod, N., Kochovski, Z., Asano, S., Vanhecke, D., Baumeister, W., and Lucic, V. (2011). Insights into the molecular organization of the neuron by cryo-electron tomography. J. Electron Microsc. (Tokyo) *60* (*Suppl 1*), S137–S148.

Fernández-Busnadiego, R., Asano, S., Oprisoreanu, A.-M., Sakata, E., Doengi, M., Kochovski, Z., Zürner, M., Stein, V., Schoch, S., Baumeister, W., and Lucić, V. (2013). Cryo-electron tomography reveals a critical role of RIM1α in synaptic vesicle tethering. J. Cell Biol. *201*, 725–740.

Frangakis, A.S., and Hegerl, R. (2001). Noise reduction in electron tomographic reconstructions using nonlinear anisotropic diffusion. J. Struct. Biol. *135*, 239–250.

Gaffield, M.A., and Betz, W.J. (2007). Synaptic vesicle mobility in mouse motor nerve terminals with and without synapsin. J. Neurosci. *27*, 13691–13700.

Gallardo, G., Schlüter, O.M., and Südhof, T.C. (2008). A molecular pathway of neurodegeneration linking alpha-synuclein to ApoE and Abeta peptides. Nat. Neurosci. *11*, 301–308.

Godino, Mdel.C., Torres, M., and Sánchez-Prieto, J. (2007). CB1 receptors diminish both Ca(2+) influx and glutamate release through two different mechanisms active in distinct populations of cerebrocortical nerve terminals. J. Neurochem. *101*, 1471–1482.

Greten-Harrison, B., Polydoro, M., Morimoto-Tomita, M., Diao, L., Williams, A.M., Nie, E.H., Makani, S., Tian, N., Castillo, P.E., Buchman, V.L., and Chandra, S.S. (2010). αβγ-Synuclein triple knockout mice reveal age-dependent neuronal dysfunction. Proc. Natl. Acad. Sci. USA *107*, 19573–19578.

Gundelfinger, E.D., Reissner, C., and Garner, C.C. (2016). Role of Bassoon and Piccolo in assembly and molecular organization of the active zone. Front. Synaptic Neurosci. *7*, 19.

Hirokawa, N., Sobue, K., Kanda, K., Harada, A., and Yorifuji, H. (1989). The cytoskeletal architecture of the presynaptic terminal and molecular structure of synapsin 1. J. Cell Biol. *108*, 111–126.

Ho, A., Morishita, W., Hammer, R.E., Malenka, R.C., and Südhof, T.C. (2003). A role for Mints in transmitter release: Mint 1 knockout mice exhibit impaired GABAergic synaptic transmission. Proc. Natl. Acad. Sci. USA *100*, 1409–1414.

Hui, E., Johnson, C.P., Yao, J., Dunning, F.M., and Chapman, E.R. (2009). Synaptotagmin-mediated bending of the target membrane is a critical step in Ca(2+)-regulated fusion. Cell *138*, 709–721.

Imig, C., Min, S.-W., Krinner, S., Arancillo, M., Rosenmund, C., Südhof, T.C., Rhee, J., Brose, N., and Cooper, B.H. (2014). The morphological and molecular nature of synaptic vesicle priming at presynaptic active zones. Neuron *84*, 416–431.

Janezic, S., Threlfell, S., Dodson, P.D., Dowie, M.J., Taylor, T.N., Potgieter, D., Parkkinen, L., Senior, S.L., Anwar, S., Ryan, B., et al. (2013). Deficits in dopaminergic transmission precede neuron loss and dysfunction in a new Parkinson model. Proc. Natl. Acad. Sci. USA *110*, E4016–E4025.

Jiang, Y.-H., and Ehlers, M.D. (2013). Modeling autism by SHANK gene mutations in mice. Neuron *78*, 8–27.

Koo, S.J., Kochlamazashvili, G., Rost, B., Puchkov, D., Gimber, N., Lehmann, M., Tadeus, G., Schmoranzer, J., Rosenmund, C., Haucke, V., and Maritzen, T. (2015). Vesicular synaptobrevin/VAMP2 levels guarded by AP180 control efficient neurotransmission. Neuron *88*, 330–344.

Kremer, J.R., Mastronarde, D.N., and McIntosh, J.R. (1996). Computer visualization of three-dimensional image data using IMOD. J. Struct. Biol. *116*, 71–76.

Lučić, V., Fernández-Busnadiego, R., Laugks, U., and Baumeister, W. (2016). Hierarchical detection and analysis of macromolecular complexes in cryo-electron tomograms using Pyto software. J. Struct. Biol. *196*, 503–514.

Martens, S., Kozlov, M.M., and McMahon, H.T. (2007). How synaptotagmin promotes membrane fusion. Science *316*, 1205–1208.

Merrifield, C.J., and Kaksonen, M. (2014). Endocytic accessory factors and regulation of clathrin-mediated endocytosis. Cold Spring Harb. Perspect. Biol. *6*, a016733.

Middleton, E.R., and Rhoades, E. (2010). Effects of curvature and composition on α-synuclein binding to lipid vesicles. Biophys. J. *99*, 2279–2288.

Nakajo, S., Tsukada, K., Kameyama, H., Furuyama, Y., and Nakaya, K. (1996). Distribution of phosphoneuroprotein 14 (PNP 14) in vertebrates: its levels as determined by enzyme immunoassay. Brain Res. *741*, 180–184.

Nemani, V.M., Lu, W., Berge, V., Nakamura, K., Onoa, B., Lee, M.K., Chaudhry, F.A., Nicoll, R.A., and Edwards, R.H. (2010). Increased expression of alpha-synuclein reduces neurotransmitter release by inhibiting synaptic vesicle reclustering after endocytosis. Neuron *65*, 66–79.

Nicholls, D.G. (2003). Bioenergetics and transmitter release in the isolated nerve terminal. Neurochem. Res. *28*, 1433–1441.

Nicholls, D.G., and Sihra, T.S. (1986). Synaptosomes possess an exocytotic pool of glutamate. Nature *321*, 772–773.

Nickell, S., Förster, F., Linaroudis, A., Net, W.D., Beck, F., Hegerl, R., Baumeister, W., and Plitzko, J.M. (2005). TOM software toolbox: acquisition and analysis for electron tomography. J. Struct. Biol. *149*, 227–234.

Penzes, P., Cahill, M.E., Jones, K.A., VanLeeuwen, J.-E., and Woolfrey, K.M. (2011). Dendritic spine pathology in neuropsychiatric disorders. Nat. Neurosci. *14*, 285–293.

Polymeropoulos, M.H., Lavedan, C., Leroy, E., Ide, S.E., Dehejia, A., Dutra, A., Pike, B., Root, H., Rubenstein, J., Boyer, R., et al. (1997). Mutation in the alpha-synuclein gene identified in families with Parkinson's disease. Science *276*, 2045–2047.

Rizzoli, S.O., and Betz, W.J. (2005). Synaptic vesicle pools. Nat. Rev. Neurosci. *6*, 57–69.

Rosahl, T.W., Spillane, D., Missler, M., Herz, J., Selig, D.K., Wolff, J.R., Hammer, R.E., Malenka, R.C., and Südhof, T.C. (1995). Essential functions of synapsins I and II in synaptic vesicle regulation. Nature *375*, 488–493.

Scott, D., and Roy, S. (2012). α-Synuclein inhibits intersynaptic vesicle mobility and maintains recycling-pool homeostasis. J. Neurosci. *32*, 10129–10135.

Scott, D.A., Tabarean, I., Tang, Y., Cartier, A., Masliah, E., and Roy, S. (2010). A pathologic cascade leading to synaptic dysfunction in alpha-synuclein-induced neurodegeneration. J Neurosci. *30*, 8083–8095.

Siksou, L., Rostaing, P., Lechaire, J.P., Boudier, T., Ohtsuka, T., Fejtová, A., Kao, H.T., Greengard, P., Gundelfinger, E.D., Triller, A., and Marty, S. (2007). Three-dimensional architecture of presynaptic terminal cytomatrix. J Neurosci. *27*, 6868–6877.

Siksou, L., Triller, A., and Marty, S.; Ultrastructural organization of presynaptic terminals (2011). Curr Opin Neurbiol. *21*, 261–268.

Singleton, A.B., Farrer, M., Johnson, J., Singleton, A., Hague, S., Kachergus, J., Hulihan, M., Peuralinna, T., Dutra, A., Nussbaum, R., et al. (2003). Alpha-synuclein locus triplication causes Parkinson's disease. Science *302*, 841.

Takamori, S., Holt, M., Stenius, K., Lemke, E.A., Grønborg, M., Riedel, D., Urlaub, H., Schenck, S., Brügger, B., Ringler, P., et al. (2006). Molecular anatomy of a trafficking organelle. Cell *127*, 831–846.

Taylor, T.N., Potgieter, D., Anwar, S., Senior, S.L., Janezic, S., Threlfell, S., Ryan, B., Parkkinen, L., Deltheil, T., Cioroch, M., et al. (2014). Region-specific deficits in dopamine, but not norepinephrine, signaling in a novel A30P α-synuclein BAC transgenic mouse. Neurobiol. Dis. *62*, 193–207.

van Spronsen, M., and Hoogenraad, C.C. (2010). Synapse pathology in psychiatric and neurologic disease. Curr. Neurol. Neurosci. Rep. *10*, 207–214.

Vargas, K.J., and Chandra, S.S. (2015). Synucleins. In Reference Module in Biomedical Sciences, M. Caplan, ed. (Elsevier), pp. 833–837.

Vargas, K.J., Makani, S., Davis, T., Westphal, C.H., Castillo, P.E., and Chandra, S.S. (2014). Synucleins regulate the kinetics of synaptic vesicle endocytosis. J. Neurosci. *34*, 9364–9376.

Wang, L., Das, U., Scott, D.A., Tang, Y., McLean, P.J., and Roy, S. (2014). α-synuclein multimers cluster synaptic vesicles and attenuate recycling. Curr. Biol. *24*, 2319–2326.

Westphal, C.H., and Chandra, S.S. (2013). Monomeric synucleins generate membrane curvature. J. Biol. Chem. *288*, 1829–1840.

Whittaker, V.P. (1993). Thirty years of synaptosome research. J. Neurocytol. *22*, 735–742.

Wilhelm, B.G., Mandad, S., Truckenbrodt, S., Kröhnert, K., Schäfer, C., Rammner, B., Koo, S.J., Claßen, G.A., Krauss, M., Haucke, V., et al. (2014). Composition of isolated synaptic boutons reveals the amounts of vesicle trafficking proteins. Science *344*, 1023–1028.